Transition from dispersive to nondispersive transport: Photoconduction of polyvinylcarbarzole

E. Muller-Horsche and D. Haarer
Physikalisches Institut and Bayreuther Institüt für Forschung, Universität Bayreuth, Postfach 3008, D-8580 Bayreuth, Federal Republic of Germany

H. Scher
Standard Oil, Research and Development, 4440 Warrensville Center Road, Warrensville Heights, Ohio 44128
(Received 2 June 1986)

Photocurrents in polyvinylcarbarzole were studied over 10 decades in time. An analytical approach is proposed for extracting rate distributions from the measured photocurrents. We find that the trapping-rate distribution is not exponential but "flat" and that it shows a cutoff at low rates. This distribution gives rise to the novel feature of a gradual transition from dispersive to nondispersive charge transport during a single transit. The temperature and field dependence of the cutoff rate r_c was studied in the framework of a Poole-Frenkel model.

I. INTRODUCTION

Pulsed photocurrents are a powerful means of investigating the dynamic parameters of amorphous materials over a large range. In this paper we will present experimental data which cover 10 orders of magnitude in time and can therefore be used to study not only the absolute values of the pertinent rates, but also draw conclusions concerning their frequency distribution.

For testing our analytical and experimental approach, we chose a well-investigated system, polyvinylcarbarzole (PVK), because we could compare our data with other experimental data and discuss the new aspects of our approach on the background of previous methods and conclusions.

It is well documented that photocurrents in polymer systems like PVK show dispersive behavior. The general theory of dispersive transport was developed by Scher and Montroll (SM).[1] In the theory, the key physical idea is that the microscopic processes which control carrier transport are governed by a distribution of event times which is broad over the time range of experimental observation. SM used the formalism of continuous-time random walk (CTRW) to describe carrier motion with an event-time distribution $\psi(t)$; the event time could either be due to, e.g., hopping between localized states or release from a trap. SM showed that for a $\psi(t)$ with a slowly varying algebraic time dependence, $\psi(t)\sim t^{-(1+\alpha)}$, with a disorder parameter α, in the range $0<\alpha<1$, one could account for *all* of the key features of dispersive transport.

Noolandi[2] and Schmidlin[3] showed that the conventional set of coupled kinetic equations describing carrier motion with repeated trapping (ω_i) and thermal release (r_i) can be cast into the framework of the CTRW and is therefore equivalent. They demonstrated the exact form of the $\psi(t)$ for multiple trapping (MT) in terms of $\{\omega_i,r_i\}$; therefore, MT is a subset of the microscopic transport processes describable by the $\psi(t)$.

Scher[4] used a simpler form of the $\psi(t)$ for MT and derived $\alpha=T/T_0$ for an exponential distribution of trapping states with a width parameter kT_0. Hence, specifying a microscopic model (hopping, trapping, etc.), which leads to a $\psi(t)$ one can calculate the transient photocurrent $I(t)$. The experimentalist is, however, especially interested in solving the inverse problem, since he is able to measure $I(t)$ and would like to draw conclusions about the transport mechanisms, density of localized states, etc.

The simplest approach to inversion is to assume a transport mechanism, most amenable to analytic treatment, e.g., MT, and see whether the $I(t)$ can be explained with physically reasonable model parameters. Recently a number of authors[5,6] have used the MT model in this mode. It should be added that the MT model can also function as a *phenomenological framework yielding useful characterization of microscopic processes in which the main source of dispersion is due to energy-level fluctuation.* Simulation studies[7] have demonstrated, e.g., that hopping between localized states with random site energies, distributed exponentially [$\rho(\varepsilon)\propto\exp(-\varepsilon/kT_0)$], also yields $\alpha=T/T_0$. The approach of Michiel and Adriaenssens[6] illustrate some of these issues. They have discretized a continuous distribution of trap states, leading to a formulation similar to Schmidlin,[3] and used simple matrix methods to determine $I(t)$. There is some arbitrariness to this procedure. One is simply generating a theoretical fit to a reasonable finite set of $\{\omega_i,r_i\}$. The intrinsic ambiguity in the discrete representation of $\rho(\varepsilon)$ is complicated by the fit to $I(t)$ only over a time range, typically of two decades. We have clarified the issue of the intrinsic resolution of the rate distribution derivable from $I(t)$ measurements.

The method, which will be presented below, is adapted to the needs of the experimentalist; in particular, it does not make assumptions about rate distributions. It can be demonstrated that the rate distributions can be extracted from the experimental data. There is a price, however, which we have to pay for making no restricting assumptions about the trap distributions. We have to perform ex-

periments, which cover many orders of magnitude in time or rate. In our case we performed experiments over 10 decades and derived rate distributions over 5–6 decades. This "loss in information" is due to comparatively broad distribution functions, which enter into our Laplace analysis. We do not want to rule out that there is a more sophisticated approach, which has a higher intrinsic resolution. Our main goal is, at the present time, to raise the issue of rate distributions, discuss our results versus the usefulness of effective mobilities μ_{eff} and to present our data for further theoretical considerations.

II. MANIPULATION OF THE SOLUTION FOR THE PHOTOCURRENT IN THE FRAMEWORK OF THE MULTIPLE TRAPPING MECHANISM

In our mathematical description of the photocurrent we use the treatment of the multiple trapping model as has been formulated by Schmidlin:[3]

$$\begin{aligned}\frac{\partial p(z,t)}{\partial t} &= q(z,t)+\sum p_i(z,t)r_i - p(z,t)\sum_i \omega_i \\ &\quad -\frac{\partial}{\partial z}p(z,t)\mu E(z,t)\ , \\ \frac{\partial p_i}{\partial t} &= p\omega_i - p_i r_i\ .\end{aligned} \tag{1}$$

The trapping rates ω_i and detrapping rates r_i populate and depopulate the charge densities $p(z,t)$ and $p_i(z,t)$ in the conduction band and in the traps, respectively. The function $q(z,t)$ stands for the rate of charge carrier production. $\partial(p\mu E)/\partial z$ describes the process of charge accumulation by a gradient in the local flux. In the following we assume that space-charge effects can be neglected and, hence, we assume a constant electric field across the sample (see Fig. 1).

Assuming pulsed excitation in our sample with light of an infinitely short penetration depth we have

$$q(z,t)=N\delta(z-0)\delta(t-0)\ ,$$

and for this special case the Laplace transform of the total current $I(t)$ can be calculated as

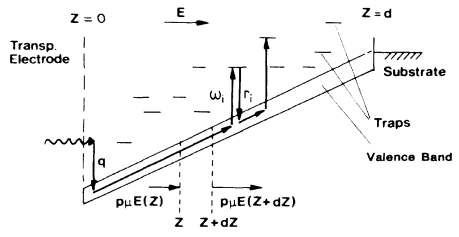

FIG. 1. Multiple trapping parameters (for holes); q is the carrier production term, ω_i the trapping rate, r_i the detrapping rate, E the electric field, d the sample thickness, p the carrier density, and z is the integration coordinate (see Ref. 3).

$$\tilde{I}(r)=N\frac{1-\exp[-a(r)t_0]}{a(r)t_0}\ . \tag{2}$$

$t_0=d/\mu E$ stands for the microscopic transit time, i.e., the transit time of a fictive charge carrier which remains in the band as a free carrier as it traverses the sample of thickness d under the influence of a field E. The quantity $a(r)$ contains the rate variable r in Laplace space as well as the trapping and detrapping rates ω_i and r_i,

$$a(r)=r\left[1+\sum_i \frac{\omega_i}{r+r_i}\right]\ , \tag{3}$$

it is proportional to $\tilde{\psi}^{-1}(r)$, where $\tilde{\psi}$ is the Laplace transform of $\psi(t)$.

In our experiments we obtained $I(t)$ in digitized form and the Laplace transform $\tilde{I}(r)$ could be calculated numerically. Thus, $\tilde{I}(r)$ can be regarded as the experimental input for the subsequent mathematical procedures.

If one extrapolates Eq. (2) to $r\to 0$, one obtains the total charge contributing to the photocurrent

$$\tilde{I}(r\to 0)=N\ .$$

This presumes that the initially generated charge carriers N are entirely contained in the conduction band (no initial occupation of the traps). N can be used to normalize $\tilde{I}$,

$$\tilde{I}/N=\frac{1-\exp(-at_0)}{at_0} \tag{4}$$

so that $a(r)t_0$ can be gained from the experimental data $\tilde{I}/N$ by inversion of Eq. (4). This is done by finding the roots of the following equation using the Newton method:

$$\tilde{I}/N-\frac{1-\exp(-at_0)}{at_0}=0\ .$$

The microscopic mobility μ, contained in the proportionality factor t_0, is approximated from the value of the peak current at each field E. Due to the instrumental time resolution (~ 10 ns), this procedure yields a lower limit for μ. This, in turn, leads to a least upper bound for the rate spectrum we can analyze (see below). Note, that $a(r)$ [Eq. (3)] contains all the model parameters r_i and ω_i, which we like to determine. To do so, we introduce the logarithms $r^*=\ln r$ and $r_i^*=\ln r_i^*$ and rewrite Eq. (3),

$$a(r^*)t_0=e^{r^*}t_0+\sum_i M_i\frac{1}{1+e^{r_i^*-r^*}}\ . \tag{5}$$

We have also introduced the quantity $M_i=\omega_i t_0$ (number of trapping events into the ith level during the microscopic transit time t_0). Differentiation of Eq. (5) with respect to r^* yields

$$\begin{aligned}F(r^*) &:= d(at_0)^*/dr^* - e^{r^*}t_0 \\ &= \sum_i [M_i f(r_i^*-r^*)]\ .\end{aligned} \tag{6}$$

This represents a superposition of the bell-shaped curves $M_i f(r_i^*-r^*)$ centered around the detrapping rates r_i and weighted with M_i. Note that $f(x)$ is normalized to 1. Its shape is depicted in Fig. 2.

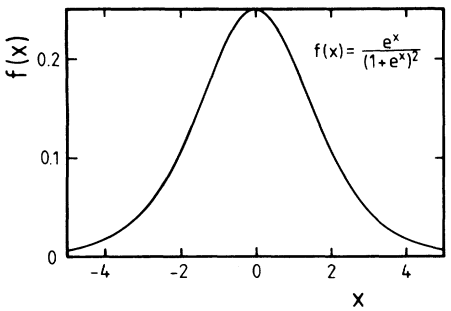

FIG. 2. $f(x)$ function limiting our resolution in the Laplace transform. The function is normalized to 1. $f(x)$, plotted on a log-log scale, will appear like a rounded-off triangle with slopes 1 on either side (see Fig. 3).

The functional dependence of the distribution $F(r^*)$, as defined in Eq. (6), on the quantities M_i and r_i suggests the following generalization to a continuum of traps:

$$F(r^*)=\int M(s^*)f(s^*-r^*)ds^* , \tag{7}$$

with the following definition of $M(r^*)$: $M(r^*)dr^*$ gives the number of trapping events during the time t_0 into traps having detrapping rates between r^* and r^*+dr^*. It is $M(r^*)$ that gives us information about the trap density through the relation $M(r^*)=t_0 b_t n(r^*)$, where b_t is the trap capture coefficient and $n(r^*)dr^*$ the trap density in the interval r^*, r^*+dr^*. One can relate $n(r^*)$ to the density of states $\rho(\varepsilon)$, once $r(\varepsilon)$ is specified (see below).

The distribution function $F(r^*)$ can be obtained from our experimental photocurrents, which yield $a(r)t_0$ [via Eq. (4)] and the definition in Eq. (6). The right-hand side of Eq. (7) corresponds to a rate distribution $M(r^*)$, which is broadened by the function f. A deconvolution of $F(r^*)$ is not very well defined because of the width of f and because of boundary problems (not included in Ref. 6). Therefore we treat $F(r^*)$ as a broadened distribution of $M(r^*)$ and try to get information from our experiments by measuring the photocurrents over many orders of magnitudes in time (e.g., 10 decades in the experimental results presented in a later section). This corresponds to a large range of available $F(r^*)$ data on the r^* scale and the larger this interval, the smaller the relative width of f. This width of $f(r^*)$ is a clearer statement of the resolution limit of using $I(t)$ as a spectroscopy tool, e.g., it corresponds to some of the ill-posed nature of the discretization of $\rho(\varepsilon)$ discussed in Ref. 6.

III. TEST OF OUR DATA ANALYSIS THROUGH NUMERICAL CALCULATIONS

In order to check the applicability of the above evaluation algorithms for obtaining densities in the parameter's space of trapping and detrapping rates, we performed numerical simulations of photocurrents based on Eq. (1). The generation term $q(z,t)$ of charge carriers was implemented by chosing the appropriate initial conditions for $p(z,0)$.

In our calculations the pertinent trapping and detrapping rates were introduced as parameters which were normalized to the inverse microscopic transit time t_0, with

$$R_i=r_i t_0 \quad \text{and} \quad M_i=\omega_i t_0 \tag{8}$$

(letting $rt_0\rightarrow r$).

For the numerical evaluation we followed Fleming and Schmidlin[3,8] and used a set of seven parameters of

$$R_i=0.01(\sqrt{10})^{i-1} , \quad i=1,2,\ldots,7$$

and

$$M_i=R_i^{0.6} . \tag{9}$$

The details of implementing the drift term of the electric field into our calculations are given elsewhere.[8,9] We also limited the number of charge carriers to a value which was low enough to neglect the influence of space charges. This was achieved by maintaining the condition

$$\int I\,dt=10^{-3}\,CU , \tag{10}$$

where I is the photocurrent, C the sample capacitance, and U the applied voltage.

Figure 3 shows in a double-logarithmic plot the product of the rates M_i broadened by the function $f(R_j^*-r^*)$ as given by a single term in Eq. (6). The width of the seven bell-shaped curves (dotted) characterizes the "resolution" of our analysis based on the Laplace transform procedure as given in Sec. II. One single set of rate parameters R_i, M_i would yield one single bell-shaped curve. The sum of the various rates $i=1,2,\ldots,7$ is depicted by the envelope function (heavy dots).

Using our numerical program for calculating the photocurrent, we arrived at the solid line, which is shown in the

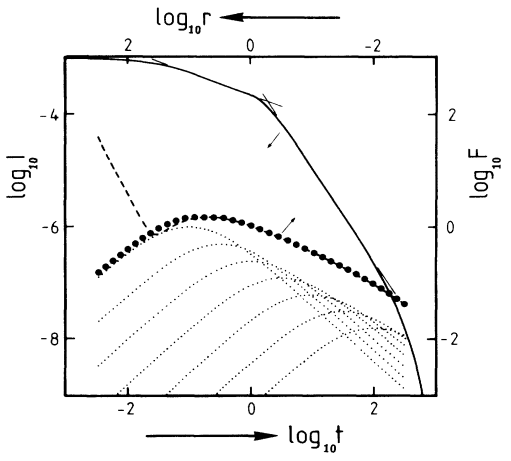

FIG. 3. Lower part: Contribution of the product functions $M_i f(R_i^*-r^*)$ (see triangular, dotted curves). The sum of the seven contributing rates is drawn by the dotted line (heavy dots); the "deconvoluted" rate distribution (see text) is given by the dashed line. (The arrows point in the direction of the axes.) Upper part: Photocurrent $I(t)$ (solid line) calculated from the original rate distribution (heavy dots). Note that the exponents agree with the predictions of the CTRW theory (the falloff at long times is due to the arbitrary cutoff of the given rate distributions).

upper part of Fig. 3. This photocurrent was then taken as the starting point for checking the quality of our Laplace analysis. The flow diagram as given in Fig. 4 was taken to reproduce the rate density as given by Eq. (6).

For the given example the evaluation scheme reproduces the initial rate distribution well for rates $r<40$ (in units of $1/t_0$). For rates $r>40$ the procedure of deconvoluting the photocurrent with our method fails (see Fig. 3). This is, in our opinion, due to the fact, that the numerical subtraction, as given by Eq. (6), becomes ill defined. Here one has to subtract two large expressions, namely, $d(at_0)/dr^*$ and $\exp(r^*)t_0$. Both terms have comparable magnitude and their difference yields the $F(r^*)$ function. When analyzing our experimental data in the following section, we have to limit our analysis to rates which are smaller than $10/t_0$. Since t_0 turns out to be on the order of 20 μs, our analysis will work rather well below rates of $5\times10^5\ s^{-1}$.

It should be mentioned, that our calculation of the photocurrent reproduces the predictions of the CTRW theory rather well: The slopes of the calculated photocurrent (Fig. 3) come close to the predicted values of $\alpha=-(1\pm0.6)$ as can be expected after using the ansatz $M_i=R_i^{0.6\ldots3}$.

Our calculation gives us a convenient tool to also investigate the influence of space-charge effects. Figure 5 gives a corresponding calculation of the photocurrent I belonging to an identical rate distribution, but with an injected charge which is 500 times larger [$0.5CU$, see Eq. (10)]. It is evident that the Laplace evaluation scheme is not as consistent as it is for negligible space charges. Here the deconvoluted rate distribution differs from the initial distribution for rates $r>1$, thus reducing the range in which self-consistency can be achieved with our model. Before evaluating our experimental data one can summarize the main features of our evaluation scheme: We can extract

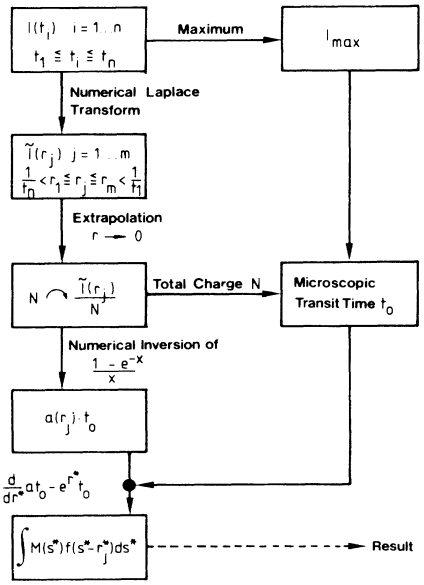

FIG. 4. Calculational procedure of our Laplace convolution method (see text).

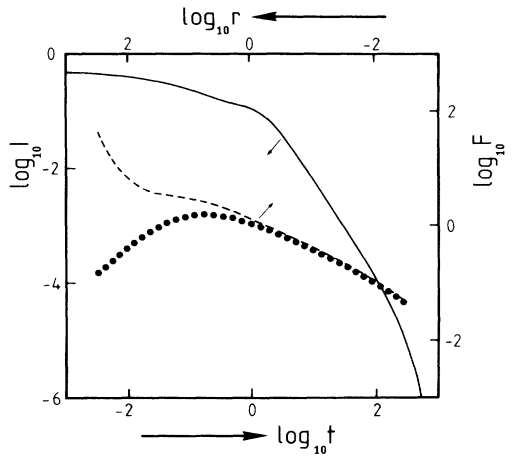

FIG. 5. Initial rate distribution (heavy dots), photocurrent (solid line), and deconvoluted rate distribution (dashed line). The calculation was performed under moderate space-charge conditions (see text) and, thus, gives less self-consistency.

trapping rate distributions from a given photocurrent for detrapping rates smaller than $10/t_0$, where t_0 is the microscopic transit time. Within this limit the procedure is self-consistent. Our model calculations show one intrinsic limitation. Since the functional dependence of $F(r^*)$ characterizing one set of rates R_i and M_i is rather broad (see dotted inserts in Fig. 3) we believe, that a meaningful data analysis has to exceed the time range of 6 orders of magnitude, in order to yield substantial information about rate distributions. Therefore we have taken a great deal of effort to cover a time range of about 10 decades in order to extract information about rate distributions, which are reliable over 5—6 orders of magnitude.

IV. EXPERIMENTAL RESULTS

As samples we used commercial PVK (102, Luvican, trade name BASF) which was purified by repeated precipitation from solution and which contained less than 0.05% monomer carbazole. The films were cast from THF solution. To maintain a well-defined sample thickness, we used a technique in which a spatula could be moved parallel to a precision surface with an accuracy of $<1\ \mu$. The substrate onto which the films were spread was mylar coated with a thin Al layer. The evaporation rate of the solvent after the spreading procedure could be optimized by casting the films in a glove box with variable gas flow. (There was no measurable difference in sample quality comparing inert gas and air.) After air drying the samples were annealed at 80 °C for 30 min to remove the residual solvent.

A typical sample thickness was 10 μm. As the second electrode we used a thin layer of semitransparent, evaporated aluminum. Contacts to both aluminum surface layers were formed in a way which is schematically shown in Fig. 6. The additional layer of insulating varnish on the side of the sample, at which the top electrode was con-

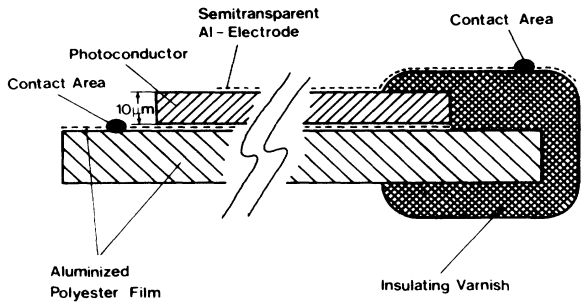

FIG. 6. Cross section through the sample between two aluminum electrodes. The insulating varnish covering the right edge of the sample was introduced as a means to prevent breakdown.

tacted, was implemented to prevent breakthrough problems along the edges of the sample.

As a light source we used a pulsed nitrogen laser with a pulse energy of about 5 mJ at the wavelength 337 nm. The pulse width was 10 ns. With the above excitation conditions, the penetration depth of the light was < 0.2 μm, i.e. about 50 times less than the sample thickness. This provided adequate conditions for surface excitation, i.e., for justifying a δ-function-like charge carrier distribution for our calculations at $t=0$.

One of the major challenges of the experiment was to measure currents in the time domain of 1 ns to 10 s with a maximum sensitivity of 10^{-10} Å. There is no single transient recorder which would provide a large enough dynamic range, therefore we subdivided each curve into five segments which were measured in subsequent experiments. The fast decay was monitored with a Tektronix 7912 digitizer (risetime 1 ns) and the slow part of the decay was monitored with a logarithmic time sweep (for details see Ref. 9). In the "long-time regime" we also used an amplifier with logarithmic conversion. The various sections of the decay curve were digitized; the linear sections of the decay curve were converted to log scales. The complete decay curve was subsequently displayed on a screen as depicted in Fig. 7. The figure also shows the limits of the various individual decay sections.

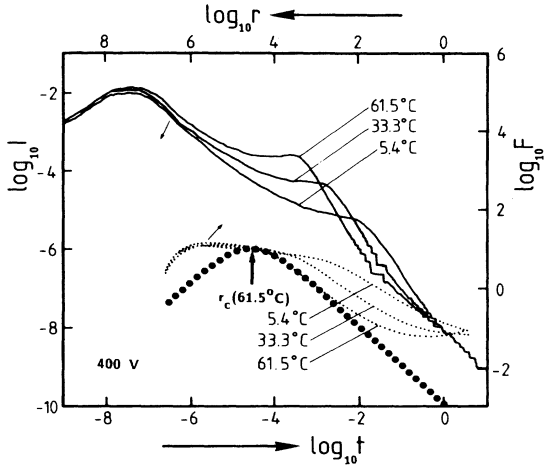

FIG. 8. Solid lines: Photocurrent of PVK (10 μm thick) at constant voltage (400 V) and variable temperature. The experimental data cover ten decades (left and lower axis). Dotted lines: Rate distributions as calculated by our Laplace transform (right and upper axis). Note, that for short times (fast rates) the validity of our evaluation scheme breaks down in the μs region (see text). The arrows point into the directions of the axes. The dotted line (heavy dots) gives the contribution of one rate r_c (61.5 °C 400 V).

Using the above-described setup, we were able to measure the photocurrent in our PVK sample over ten decades in time and over more than eight decades in intensity. Figures 8 and 9 show our results as a function of sample temperature and electric field strength.

First we used the data of Figs. 8 and 9 to evaluate the effective mobilities as defined by

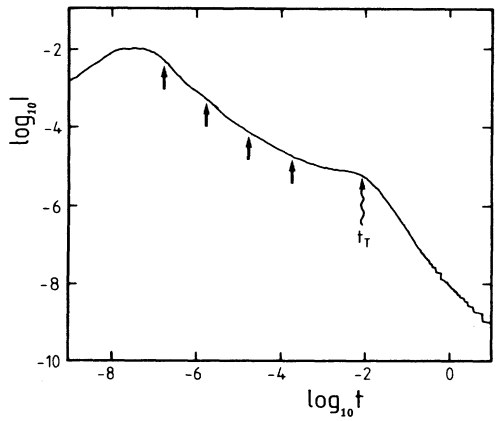

FIG. 7. Typical experimental photocurrent; the arrows mark the limits of five individual measurements, which are joined to a single curve (see text). The wavy arrow marks the transit time t_T; here the influence of the back electrodes leads to a dropoff in current.

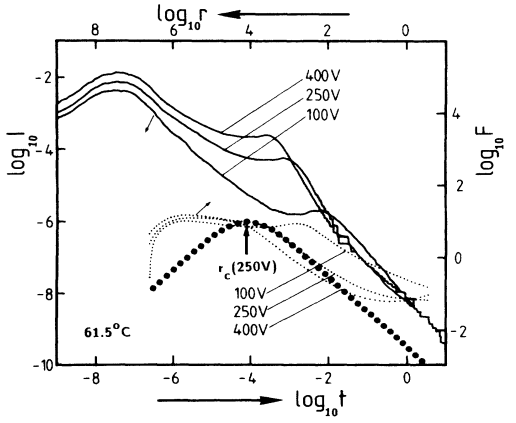

FIG. 9. Solid lines: Photocurrent of PVK (10 μm thick) at constant temperature (61.5 °C) and variable field strength. Dotted lines: Rate distribution as calculated by our Laplace transform. The dotted line (heavy dots) gives the contribution of one rate r_c (61.5 °C, 250 V).

$$\mu_{\text{eff}}=(d^2/t_T)U \ . \tag{11}$$

d is the sample thickness and t_T is the effective transit time, as taken from the experimental decay curves (see Fig. 7).

If we follow previous publications by plotting $\ln(\mu_{\text{eff}})$ versus $1/T$ (Refs. 10 and 11), we get straight lines for each temperature cycle, yet, the various curves, belonging to different field strengths, do not intersect at $1/T=0$, but at a finite temperature (see Fig. 10). Note, that in a simple model, the lines should intersect at $1/T=0$ and yield the "band mobility," i.e., the mobility in the absence of trapping (see Refs. 10 and 11). If we adopt the empirical procedure of introducing an effective temperature T', with

$$1/T'=1/T-1/T^* \tag{12}$$

we obtain an intersection point at the temperature $T^*=540$ K and a value for the effective band mobility of $\mu_{\text{eff}}=0.02$ (cm^2/Vs).

In the past this behavior of effective mobilities was attributed to a temperature dependence of the dielectric constant.[12] Our numerical analysis of the data would require a comparatively strong temperature dependence of the dielectric constant to support the above assumption (about 40% increase with $\Delta T=+50$ K).

Proceeding with the above arguments, one can express the effective mobility μ_{eff} as a function of the electric field strength by assuming a field-dependent barrier height and get

$$\mu_{\text{eff}}=\mu_0 \exp[-\varepsilon(E)/kT'] \ , \tag{13}$$

where $\varepsilon(E)$ is the field-dependent activation energy. If we assume that a Poole-Frenkel mechanism is responsible for lowering the barrier height, then we get

$$\varepsilon(E)=\varepsilon_0-\beta\sqrt{E} \ . \tag{14}$$

Here ε_0 is the barrier height in the absence of a field and β is a nonadjustable parameter of 4.4×10^{-4} $e\sqrt{\text{V cm}}$.

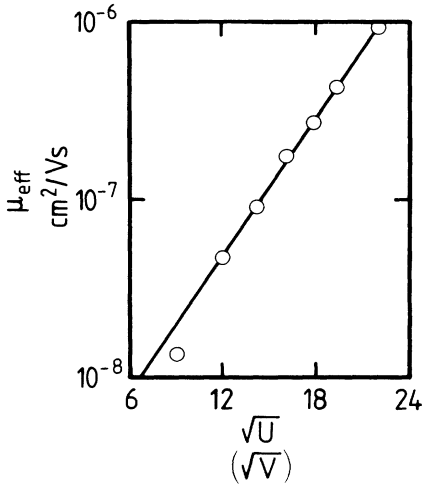

FIG. 11. Field dependence of the effective mobility in a Poole-Frenkel picture (see text).

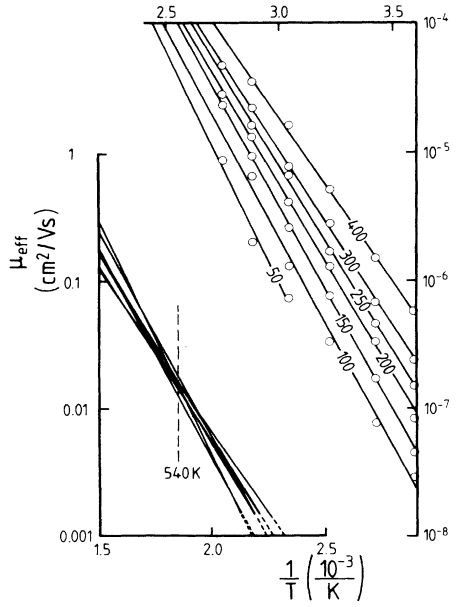

FIG. 10. Effective mobility as measured by the transit time, plotted vs $1/T$. Note, that the straight lines intersect at 540 K. (For the sake of saving space, the figure is subdivided into two sections.) The numbers label the applied voltages.

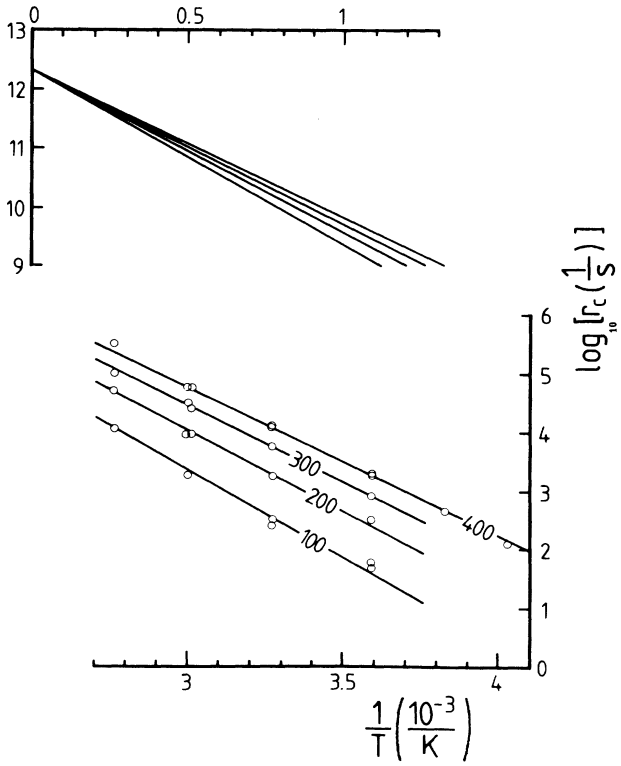

FIG. 12. Slowest rate r_c, as obtained by our rate analysis, plotted vs $1/T$. Note, that the straight lines intersect at $1/T=0$. (For the sake of saving space the figure is subdivided into two scctions.) The numbers label the applied voltages.

Our experimental data (Fig. 11) yield $\varepsilon_0=0.64$ eV and $\beta=2.4\times10^{-4}$ $e\sqrt{\text{V cm}}$, i.e., the β value is about a-factor-of-2 off from the theoretical value.

At this point we can summarize our results with the conclusion, that we get moderate agreement with semiempirical theories, describing the field and temperature dependence of the effective mobility. Above all, we do not see a convincing argument for maintaining the concept of an effective temperature T' to accommodate our data on a $1/T'$ plot.

In the remainder of the paper we focus our attention on the distribution function of trapping rates, as obtained by our Laplace algorithm. Figures 8 and 9 show the rate distribution, which we were able to extract from our data in the range between 10^6 s^{-1} to 1 s^{-1}, i.e., over about six decades. This is a large range scaled on presently available data; it is, however, a small range, compared to our experiments, which cover ten decades. This is a consequence of the low intrinsic resolution of our Laplace evaluation scheme (see Fig. 3), yet, it gives us enough information to draw several important conclusions: First, the rate distribution does not follow an exponential behavior as has been assumed for our model calculations (see Fig. 3). It seems to be rather flat over several orders of magnitude and then fall off towards lower rates at the critical lowest rate r_c. This rate is marked on Figs. 8 and 9 for the 61.5 °C curve. The falloff of the rate distribution is given by the falloff of our resolution function (slope 1 in a log-log plot). Second, the lowest rate r_c shows a typical temperature and field dependence; it decreases for lower temperatures and increases for higher fields. This interesting behavior encouraged us to evaluate the observed minimal rates r_c on a $1/T$ plot. We investigated the following ansatz:

$$\ln r_c = \ln\nu - \varepsilon(E)/kT \ . \tag{15}$$

Figure 12 shows, that if we plot the data in the above manner, we get straight lines which intersect at $1/T=0$. At this intersection point, we obtain a frequency ν of 2×10^{12} s^{-1}, which we can interpret as an "attempt-to-escape" frequency. This frequency is close to values, which have been discussed earlier.[11]

Going a step further in this interpretation, we can check the validity of a Poole-Frenkel interpretation of the measured field dependence. Figure 13 shows the dependency of the rates r_c on the square root of the applied voltage. From the figure we get a straight line with an ε_0 of 0.69 eV and with a β value of 3.4×10^{-4} $e\sqrt{\text{V cm}}$. This value is rather close to the theoretical value of 4.4×10^{-4} $e\sqrt{\text{V cm}}$ (see above). In a forthcoming publication[13] we will show that the observed temperature and field dependence of the effective mobility can be modeled under the assumption that Eqs. (15) and (14) hold for all traps, so that the introduction of an effective temperature T' (12) can be avoided.

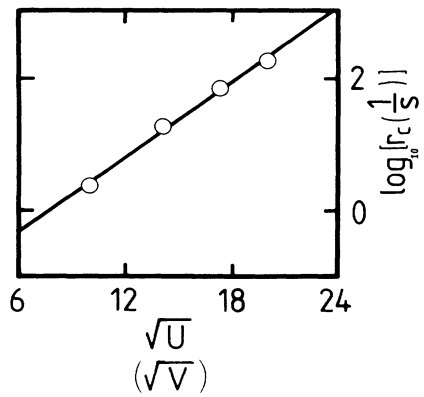

FIG. 13. Poole-Frenkel plot of the slowest rate r_c (see text).

The field dependence in Eq. (14) can also be understood as Coulomb effect in a charge transfer step between localized molecular states. If the microscopic mobility is due to hopping, the hole can be trapped in a lower ionization energy state, forming a cation and detrapped when an electron transfers up from a neutral molecule, leaving behind a cation.

V. DISCUSSION AND SUMMARY

Based on our experimental data we come to the conclusion that the distribution of trapping rates is flat over the parameter range $r < 10^{-6}$ s^{-1} which we can evaluate experimentally. At a critical minimal rate r_c the distribution of rates falls off with the resolution of our Laplace transform analysis.

The large time range of the experiment has enabled us to encompass these two distinct features of the trapping rate distribution. These features cause a transition in $I(t)$ from a highly dispersive transport to an essentially nondispersive one. This type of transition has been observed in both *a*-Se (Ref. 14) and *a*-Si:H,[15] however, as a *function of T*. The transition in $I(t)$ observed in Fig. 7 occurs within a single transit time. The form for $I(t)$ for $t<t_T$ for dispersive transport[1] is

$$I(t)\propto t^{-(1-\alpha)}, \quad t<t_T \ . \tag{16}$$

We can characterize the transition in Fig. 7 as one in which $\alpha\simeq0.0$ for $-7.1<\log t<-5.25$ and $\alpha\rightarrow1.0$ for $\log t<-2.4$. The change of slopes is gradual—nearly three decades.

We will show that a characterization of $I(t)$ with a time dependent $\alpha(\log t)$ can lead directly to an approximate form for $\rho(\varepsilon)$, which is in agreement with our more accurate determination of $F(r)$.

The MT model is a particularly simple mechanism for generating an algebraic $\psi(t)$ as it involves the independent sampling of a single random variable ε (the trap energy) with a general distribution $\rho(\varepsilon)$. An excellent approximation to $\psi(t)$ for MT, in the repeated trapping and release time range, i.e., $r\tau\ll1$, $\tau^{-1}\equiv\sum_i\omega_i$, is

$$\psi(t)=\sum_i \tau\omega_i r_i e^{-r_i t} \tag{17}$$

(cf. the derivation in Secs. 2.3 and 2.4 in Ref. 4), the weighted sum of the probability per unit time to be released from the ith level. One can immediately derive $\alpha=T/T_0$, as was first done using Eq. (17) (Ref. 4) for $\rho(\varepsilon)\propto\exp(-\varepsilon/kT_0)$ and also derive the form of $\psi(t)$ for a finite width $\rho(\varepsilon)$ with a minimum r_c cutoff [Eqs. (43)

and (44) of Ref. 4]. An interesting interpretation has been made of the form of $\psi(t)$ in Eq. (17). Shlesinger[16] has introduced the notion of fractal time in analogy with a spatial RW occurring on all length scales. Shlesinger distinguishes each level or hierarchy with a multiplicative (power-law) weighting,

$$\psi(t)=\frac{1-a}{a}\sum_{n=1}^{\infty}a^n b^n \exp(-b^n t) \tag{18}$$

and for $b<a<1$ one has $\psi(t)\propto t^{-1-\alpha}$, with

$$\alpha=\frac{\ln a}{\ln b}\ . \tag{19}$$

We can generate the continuum version of Eq. (19) for the MT model by rewriting

$$\alpha=\frac{T}{T_0}=\frac{-\varepsilon/kT_0}{-\varepsilon/kT}=\frac{\ln[\rho(\varepsilon)/\rho_0]}{\ln[r(\varepsilon)/\nu]}\ , \tag{20}$$

where $r(\varepsilon)=\nu\exp(-\varepsilon/kT)$ is the release rate at the effective energy ε, which can include field-induced barrier lowering. For a general $\rho(\varepsilon)$ we conjecture that

$$\alpha(\ln t)=\frac{\ln[\rho(\varepsilon_d)/\rho_0]}{\ln[r(\varepsilon_d)/\nu]}\ , \tag{21}$$

where

$$\varepsilon_d=kT\ln(\nu t)\ , \tag{22}$$

the time-dependent demarcation energy.[17] In Eq. (21) we have a direct relation between the slope parameter of $I(t)$ and the density of states. We have calculated $\rho(\varepsilon)$ using Eq. (21) and the time-dependent tangent to the $[\log I(t)]$-$(\log t)$ curve in Fig. 7 (the details will be given elsewhere). The expression in Eqs. (14) and (15) has been used for $r(\varepsilon)$ (ε_0 denotes the field-independent part of ε). The general feature of the density of states are as follows: (1) $\rho(\varepsilon)$ is flat ($T_0\gg T$) for $\varepsilon_0<0.61$ eV; (2) a slow rollover occurs for $0.61<\varepsilon_0<0.64$ eV with an average $T_0=80$ meV; (3) between 0.65 and 0.69 eV the average $T_0=50$ meV; (4) at $\epsilon_0>0.69$ eV there is a very sharp cutoff of $\rho(\epsilon)$, with the effective $T_0\ll T$. These features, derived from Eqs. (21) and (22), are in very good agreement with the more accurately determined $F(r)$ of Fig. 8, and the value of $\varepsilon_0=0.69$ eV (Fig. 13) for r_c. The gradual change from highly dispersive to nondispersive transport corresponds to a quasiexponential range of $\rho(\varepsilon)$ ($82\geq T_0\geq 47$ meV) with an energy range nearly 0.1 eV wide. The validity of Eqs. (21) and (22) has the same range as the simpler, more intuitive treatment of MT in Ref. 17. The approach of Ref. 17 would yield similar results for $\rho(\varepsilon)$, derived from our $I(t)$ data. However, Schiff (Ref. 5) has cautioned that there are $\rho(\varepsilon)$, e.g., nonmonotonic ones, that would lead to $I(t)$ features, using the method of Ref. 17, in disagreement with experiment. One purpose of the present paper is to present a *general* procedure to extract a rate spectrum from $I(t)$ data and show the intrinsic resolution of this deconvolution.

The nearly nondispersive transport usually ascribed to PVK occurs over a time range less than 2 decades prior to t_T. If one restricts measurement of $I(t)$ to this time range than one would conclude that there is a very narrow range of trap energies instead of the broad one with a cutoff determined in the present study. The release rate r_c at the cutoff, dominates μ_{eff}, and may be a better characterization of the transport properties of PVK.

In conclusion, we would like to point out that more data over a comparable interval of rates should be made available to be able to draw more general conclusions than the ones we have suggested for the PVK system.

ACKNOWLEDGMENTS

We would like to acknowledge the support of the BASF Corporation for preparing the polymer films and for providing the polymer materials. We also would like to acknowledge the contributions of H. Domes to the numerical calculations simulating the photocurrents. This work was supported by the Deutsche Forschungsgemeinschaft (Bonn, Germany) as part of the Sonderforschungsbereich No. SFB-213.

[1]H. Scher and E. W. Montroll, Phys. Rev. B **12**, 2455 (1975).
[2]J. Noolandi, Phys. Rev. B **16**, 4466 (1977).
[3]F. W. Schmidlin, Phys. Rev. B **16**, 2362 (1977).
[4]H. Scher, in Proceedings of the Seventh International Conference on Amorphous and Liquid Semiconductors, Edinburgh, 1977 (unpublished), p. 209; G. Pfister and H. Scher, Adv. Phys. **27**, 747 (1978) (referred to in text for sections and equations).
[5]H. Michiel, J. M. Marshall, and G. I. Adriaenssens, Philos. Mag. B **48**, 187 (1983); E. A. Schiff, in *Tetrahedrally-Bonded Amorphous Semiconductors*, edited by D. Adler and H. Fritzsche (Plenum, New York, 1985), p. 357.
[6]H. Michiel and G. I. Adriaenssens, Philos. Mag. B **51**, 27 (1985).
[7]M. Silver, G. Schönherr, and H. Bässler, Phys. Rev. Lett. **48**, 352 (1982).
[8]R. I. Fleming, J. Appl. Phys. **50**, 8075 (1979).
[9]E. Muller-Horsche, Ph.D. thesis, Universität Bayreuth, 1985 (unpublished).
[10]W. D. Gill, J. Appl. Phys. **43**, 5033 (1972).
[11]M. Jujino, H. Mikawa, and M. Yokoyama, J. Non-Cryst. Solids **64**, 163 (1984).
[12]J. Hirsch, J. Phys. C **12**, 321 (1979).
[13]H. Domes, D. Haarer, and E. Muller-Horsche (unpublished).
[14]G. Pfister, Phys. Rev. Lett. **36**, 271 (1976).
[15]T. Tiedje, J. M. Cebulka, D. L. Morel, and B. Abeles, Phys. Rev. Lett. **46**, 1425 (1981).
[16]M. Shlesinger, J. Stat. Phys. **36**, 639 (1984).
[17]T. Tiedje and A. Rose, Solid State Commun. **37**, 49 (1981); J. Orenstein, M. Kastner, and V. Vaninov, Philos. Mag. B **46**, 23 (1982).